AIP | The Journal of Chemical Physics

Bidirectional mapping between self-consistent field theory and molecular dynamics: Application to immiscible homopolymer blends

Thomas D. Sewell, Kim Ø. Rasmussen, Dmitry Bedrov, Grant D. Smith, and Russell B. Thompson

Citation: The Journal of Chemical Physics **127**, 144901 (2007); doi: 10.1063/1.2776261
View online: http://dx.doi.org/10.1063/1.2776261
View Table of Contents: http://scitation.aip.org/content/aip/journal/jcp/127/14?ver=pdfcov
Published by the AIP Publishing

Bidirectional mapping between self-consistent field theory and molecular dynamics: Application to immiscible homopolymer blends

Thomas D. Sewell and Kim Ø. Rasmussen
Theoretical Division, Los Alamos National Laboratory, Los Alamos, New Mexico 87545, USA

Dmitry Bedrov and Grant D. Smith
Department of Materials Science and Engineering, University of Utah, Rm. 304, Salt Lake City, Utah 84112, USA

Russell B. Thompson
Department of Physics & Astronomy, University of Waterloo, Waterloo, Ontario N2L 3G1, Canada

(Received 19 June 2007; accepted 2 August 2007; published online 8 October 2007)

A bidirectional mapping scheme that bridges particle-based and field-based descriptions for polymers is presented. Initial application is made to immiscible homopolymer blends. The forward mapping (upscaling) approach is based on the use of molecular dynamics simulations to calculate interfacial density profiles for polymer molecular weights that can be readily relaxed using standard simulation methods. These profiles are used to determine the optimal, effective interaction parameter that appears in the one-parameter self-consistent field theory treatment employed in the present work. Reverse mapping from a field representation to a particle-based description is accomplished by the application of a density-biased Monte Carlo method that generates representative chain configurations in the blend using statistical weights derived from fields obtained from self-consistent field theory. © *2007 American Institute of Physics*.
[DOI: 10.1063/1.2776261]

I. INTRODUCTION

Based on generally accepted defining characteristics of a complex system, most polymers or polymer-containing materials of any practical interest are complex, multiscale objects. Indeed, most of the hallmarks of complexity apply to individual polymer chains of any significant length and/or interesting topological structure; let alone polymer blends, di-, tri-, or multiblock copolymers, or composite materials containing such constituents. Nevertheless, the application of theoretical scaling and renormalization group concepts have been quite useful in providing a theoretical basis for understanding the generic static and dynamic properties of polymers and polymer-containing systems. A much more difficult challenge, even for "simple" polymers, is to include the subtle differences between, say, poly(ethylene) and poly(deuteroethylene) which are known experimentally[1] to undergo phase segregation. Useful reviews that emphasize various aspects of this scientifically challenging and technologically relevant problem have been written in recent years.[2,3]

Any practical, yet chemically specific, description of the constitutive response of a given polymeric material requires a sequence of upscaling or homogenization steps, each of which entails capturing in a physically consistent manner the information that must be included in the successively larger-scale abstraction of the material. Among these are three upscalings that, in order of increasing spatiotemporal scale, (1) retain much of the "chemical" features of the system while significantly reducing the number of explicit degrees of freedom,[4,5] (2) resort to coarse graining on the scale of the persistence length of the chains,[6,7] (3) yield a mesoscopic continuum level, yet reversible-mappable (explicitly or statistically) description of the system (e.g., self-consistent field theory[8]), and finally, (4) a homogenization process that averages over the short-to-medium wavelength properties obtained from these "subscale" descriptions to yield an effective, macroscopic constitutive model suitable for use in engineering-scale calculations. Clearly, a convincing application of any such multiscale modeling methodology must include both self-consistent validation and verification among the various levels abstraction,[9] as well as comparison to experiment.

In general, *ab initio* generation of realistic chain configurations within nontrivial microphase segregated morphologies is restricted to simple primary chain structures and molecular weights below the entanglement length, due to the enormous disparity in physical relaxation/equilibration times for systems that do not satisfy those restrictive criteria and the time scales accessible to present particle-based simulation tools (i.e., molecular dynamics or Monte Carlo). Thus, if we are to use particle-based methods to study entangled polymeric systems and/or complicated morphologies, we must develop reverse mapping (downscaling) methods that project mesoscopic morphology and chain statistical properties onto specific initial conditions. Considerable progress has been made in this regard.[10–12] However, in order to be practically useful, one must also possess the means to perform forward mapping,[13] in which the essential information required by the next-higher-scale description is extracted from the results of a finer-scale simulation. Thus, what is really needed is a *bidirectional* mapping methodology, with sufficient validation for conditions amenable to direct

simulation/prediction at both scales to yield confidence in predictions made using the higher-scale theory for input to the finer-scale treatment.[14,15]

In the present work, we focus on the development of a particular bidirectional scale bridging, namely, the one between coarse-grained molecular dynamics (MD) simulations and self-consistent field theory (SCFT) in which the only adjustable parameter is the effective "Flory-Huggins" interaction parameter χ.[16] The objectives of our work are (1) to develop and demonstrate a *practical* means for extracting information from MD simulations to define an effective χ value for use in SCFT that reproduces the salient features obtained from the MD simulations (forward mapping), (2) to use this MD-based effective χ parameter to generate ensembles of representative chain configurations based on Monte Carlo sampling from the SCFT field monomer densities (reverse mapping), and (3) to validate the system configurations thus generated by direct comparison to the results of well equilibrated MD simulations.

We focus in the present work on immiscible homopolymer blends and, for purposes of method validation, chain lengths below the entanglement threshold, for which MD simulations can reliably yield well equilibrated melt configurations. The main criterion for the forward mapping is concurrence between MD- and SCFT-based interfacial widths and local concentration gradients as functions of polymer chain length and interaction potential parameters. In the case of reverse mapping, the principal criterion is agreement between the statistical properties of reverse-mapped chains and those obtained directly from well equilibrated blends.

II. METHODOLOGIES

A. Strategy for bidirectional mapping between MD and SCFT

Our objective is to efficiently obtain an ensemble of well equilibrated, representative configurations for a homopolymer blend comprised of immiscible bead-necklace polymer chains of large molecular weight (i.e., above the entanglement molecular weight), whose generation would be impractical using conventional, brute force MD or Monte Carlo (MC) simulations. There are three steps in our approach:

(1) Perform MD simulations of bead-necklace homopolymer blends consisting of relatively short (unentangled) chains denoted A_n and B_n. Because of fast chain relaxation, conventional MD or MC simulations are capable of equilibrating and correctly sampling the phase space in these systems at reasonable computational expense. These simulations yield interfacial properties [density profiles $\rho_A(z)$ and $\rho_A(z)$, along the longitudinal axis L_z in the primary simulation cell] and statistical distributions of conformational properties of polymer chains (e.g., the radius of gyration $\langle R_g^2 \rangle$).

(2) Use results obtained in (1) to parametrize SCFT such that it optimally reproduces the interfacial width, density gradient, and chain conformational characteristics. The resultant SCFT parameters are "effective" values that are only valid at the thermodynamic condition and chain length for which the fitting was performed. However, given a set of simulations over an interval of thermodynamic conditions and chain molecular weights, one can interpolate the effective SCFT parameters to particular conditions of interest.

(3) Apply a density-biased MC sampling algorithm to perform a reverse mapping based on SCFT densities generated in (2) onto bead-necklace models. These bead-necklace configurations can then be used as initial conditions for MD simulations that sample short time dynamics, viscoelastic, and mechanical properties of the system. Presumably, the time scales accessible to MD simulations (millions of time steps) should be sufficient to validate the thermodynamic stability of the predicted chain configurations and mesoscopic morphologies.

Details concerning each step in the bidirectional mapping between MD and SCFT are provided in the following sections.

B. Molecular dynamics simulations

MD simulations were performed using a bead-necklace representation of polymer chains. Each chain consisted of n beads with diameter $\sigma=1.0$ and connected by bonds of fixed length σ constrained using a modified version of the SHAKE algorithm.[17] Two types of chains (A_n and B_n) were used to simulate homopolymer blends. Same-type bead-bead interactions (A-A and B-B) were represented by a truncated and shifted (at $r_c=2.5$) Lennard-Jones potential such that both the energy and force are zero at r_c.

$$U(r) = \begin{cases} U_{\mathrm{LJ}}(r) - (r-r_c)\left|\dfrac{dU_{\mathrm{LJ}}(r)}{dr}\right|_{r=rc} - |U_{\mathrm{LJ}}(r)|_{r=rc}, & r < r_c \\ 0, & r > r_c, \end{cases}$$

$$U_{\mathrm{LJ}}(r) = 4\varepsilon[(\sigma/r)^{12} - (\sigma/r)^6]. \tag{1}$$

The bead diameter $\sigma=1.0$ and homopolymer interaction strengths $\varepsilon_{AA}=\varepsilon_{BB}=\varepsilon=1.0$ define our fundamental length and energy scale, respectively. For the A-B bead-bead interactions, the Lennard-Jones interaction described above was augmented by a short range repulsion term given by

$$U_c(r) = -\frac{\varepsilon_{AB}}{r} f(r_c, r),$$

$$f(r_c, r) = \begin{cases} [1-(r/r_c)^2]^2, & r < r_c \\ 0, & r > r_c. \end{cases} \tag{2}$$

We restricted our study to $\varepsilon_{AB}=-0.05$. The negative sign of ε_{AB} reflects a repulsive A-B interaction and leads to an immiscible blend for a mixture with overall volume fraction $\phi_A=\phi_B=0.5$.

In this work we have investigated blends with molecular weights $n=19$, 28, 38, 57, and 76 at $T^*=k_BT/\varepsilon=1.33$ and $\rho^*=N_{\mathrm{beads}}\sigma/V=0.7$. We also studied pure polymer melts for those same thermodynamic conditions. Simulations were performed in a periodic, orthorhombic cell of size $L_x=L_y$

$=15$ and $L_z=157$, with the interface nominally perpendicular to L_z. These particular cell dimensions for the blends were chosen to minimize capillary wave effects that could occur at the interface. A reversible integration scheme[18] was used to generate trajectories in the *NVT* ensemble with integration time step $\delta t^*=(\varepsilon/m\sigma^2)^{1/2}\ \delta t=0.005$.

Initially a pure polymer melt was set up in the primary simulation cell and equilibrated over several chain relaxation times (defined as the time required for relaxation of the end-to-end vector). Next, chains with center-of-mass positions $z_{\mathrm{cm}}<0$ and $z_{\mathrm{cm}}>0$ were defined to be types B and A, respectively. A short simulation with a large (negative) value of ε_{AB} (i.e., a highly immiscible blend) led to configurations with no A beads in the B-rich phase and *vice versa*. These systems were slowly annealed to the desired values of ε_{AB} and then equilibrated over several polymer chain relaxation times. Finally, production runs of lengths of several polymer relaxation times were used for data collection and subsequent analysis.

C. Self-consistent field theory (SCFT) methodology

A practical method for predicting the morphologies of amphiphilic liquids and polymeric systems is self-consistent field theory.[19] It is a coarse-grained, mean field equilibrium statistical mechanical approach in which polymers are considered to be composed of *segments*, each of which contains a sufficiently large number of chemical monomers so that adjacent segments can be treated as uncorrelated (freely jointed) entities. Based on a chosen segment volume ρ_0^{-1}, one can assign a segmental degree of polymerization N and a segment-segment interaction parameter χ. The segment volume should be sufficiently small that the polymer can be mathematically considered a continuous space curve. For a homopolymer blend consisting of segment species A and B, each assigned the same segmental volume ρ_0^{-1}, the SCFT free energy is given by[20]

$$\frac{NF}{\rho_0 V k_B T} \approx -\phi_A \ln\left(\frac{Q_A}{V\phi_A}\right) - \phi_B \ln\left(\frac{Q_B}{V\phi_B}\right) + \frac{1}{V}\int d\mathbf{r}\{\chi N \varphi_A(\mathbf{r})\varphi_B(\mathbf{r}) - w_A(\mathbf{r})\varphi_A(\mathbf{r}) - w_B(\mathbf{r})\varphi_B(\mathbf{r})\}, \tag{3}$$

where ϕ_A and ϕ_B are the overall volume fractions of A and B segments, respectively. It is important to distinguish the volumetric volume fractions ϕ_A and ϕ_B from $\varphi_A(\mathbf{r})$ and $\varphi_B(\mathbf{r})$, which are the spatially dependent *local* volume fractions. It is these local densities that provide information concerning the mesoscopic morphology. The functions $w_A(\mathbf{r})$ and $w_B(\mathbf{r})$ in Eq. (3) are fields conjugate to the densities that incorporate the pairwise intersegmental interactions. The partition function of a single homopolymer chain subject to the field $w_{A(B)}(\mathbf{r})$ is given by $Q_{A(B)}(\mathbf{r})$. To complete the description, V is the system volume, k_B is Boltzmann's constant, and T is the temperature. The fields and densities are obtained self-consistently to minimize the free energy [Eq. (3)] using the equations (for a homopolymer blend),

$$w_{A(B)}(\mathbf{r}) = \chi N \varphi_{B(A)}(\mathbf{r}) + \xi(\mathbf{r}), \tag{4}$$

$$\varphi_{A(B)}(\mathbf{r}) = \frac{V\phi_{A(B)}}{Q_{A(B)}}\int_0^{\alpha_{A(B)}} ds q_{A(B)}(\mathbf{r},s) q_{A(B)}(\mathbf{r},\alpha_{A(B)}-s), \tag{5}$$

$$\varphi_A(\mathbf{r}) + \varphi_B(\mathbf{r}) = 1, \tag{6}$$

with

$$Q_{A(B)} = \int d\mathbf{r} q_{A(B)}(\mathbf{r},\alpha_{A(B)}). \tag{7}$$

In Eq. (5), the space curves of the polymers A and B are integrated over the chain contour parameter s from one end $s=0$ to the other $s=\alpha_{A(B)}$. For this work we will consider a symmetric polymer blend where $\alpha_A=\alpha_B=1$. The quantity $(\mathbf{r})$ in Eq. (4) is a Lagrangian multiplier used to enforce incompressibility. The propagators $q_{A(B)}(\mathbf{r},s)$ incorporate the Gaussian statistics of the chains and are obtained as solutions to the modified diffusion equation,

$$\frac{\partial q_{A(B)}(\mathbf{r},s)}{\partial s} = \frac{Na_{A(B)}^2}{6}\nabla^2 q_{A(B)}(\mathbf{r},s) - w_{A(B)}(\mathbf{r}) q_{A(B)}(\mathbf{r},s), \tag{8}$$

with $q_{A(B)}(\mathbf{r},s=0)=1$ and for which $a\equiv a_A\equiv a_B$ is the statistical segment length of the polymer chains. Note that χ and N in Eqs. (3)–(8) always appear together as the product χN. If one uses the radius of gyration of a polymer $R_g=N^{1/2}a/\sqrt{6}$ as the unit of distance in the theory, then $Na^2/6$ disappears from Eq. (8). Thus, the only remaining parameters are χN and ϕ_A (or $\phi_B=1-\phi_A$). Since we are considering a symmetric blend, we have $\phi_A=\phi_B=0.5$ which leaves χN as the only adjustable parameter, which we will use to map between SCFT and MD simulations. We employ a real-space approach introduced by Drolet and Fredrickson[21] to solve the system of equations given by Eqs. (4)–(6). Details of the implementation can be found in Refs. 22 and 23.

D. Generation of representative configuration using SCFT

From SCFT we obtain the spatial segmental distributions of chains in the equilibrium state. For a chain of N segments, the local volume fraction of segment i is

$$\varphi_i(\mathbf{r}) = \frac{V\phi_{A(B)}}{Q}\int_{s_i}^{s_{i+1}} ds q(\mathbf{r},s) q(\mathbf{r},\alpha_{A(B)}-s), \tag{9}$$

where $s_i(s_{i+1})$ is the beginning (end) of the ith segment. The volume fraction can also be thought of as the probability that the ith segment can be found at position $\mathbf{r}$. This interpretation can be used to generate representative chain configurations appropriately distributed in space using the density-biased Monte Carlo method, as was proposed by Aoyagi *et al.*[10] Specifically:

(1) The first segment of a chain is placed by randomly choosing a point $\mathbf{r}$ within the simulation box, and the local volume fraction $\varphi_1(\mathbf{r})$ for the first segment is then

compared to a random deviate p uniformly distributed in the interval [0,1). If $p \leqslant \varphi_1(\mathbf{r})$, the segment is positioned at $\mathbf{r}$ and we proceed to (2) defined below; otherwise (1) is repeated until an acceptable chain origin is obtained.

(2) Assuming that the ith segment of the chain has been placed at $\mathbf{r}'$, we randomly select a point $\mathbf{r}$ on the sphere $|\mathbf{r}-\mathbf{r}'|=a$, where a is the segmental length defined previously. As before, the $(i+1)$th monomer is placed at $\mathbf{r}$ if $p \leqslant \varphi_{i+1}(\mathbf{r})$; otherwise step (2) is repeated until a statistically valid position for the $(i+1)$th segment is obtained.

Steps (1) and (2) are repeated to generate any desired number of chains within the simulation cell (with appropriate application of periodic boundary conditions).

Clearly, this procedure has no mechanism to avoid overlapping of segments or ensure correct intermolecular correlations, since segments with $|i-j|>1$ or belonging to different chains lack any "knowledge" of the position of previously placed segments. Therefore, complete neglect of excluded volume between segments can result in significant perturbation of chain conformations after the bead-spring model has been imposed (reverse mapped) onto these freely jointed chain configurations. This recently identified issue for mapping between freely jointed and bead-spring models in polymer melts[24] has been overlooked in the past[25] as well as in recent works.[10] Thus, generation of representative configurations using density-biased Monte Carlo should be modified to include (at least partially) the excluded volume interaction in order to avoid artificial chain configurations in the reverse mapping procedure. Detailed discussion of this issue as well as modifications of the basic chain generation procedure are presented in the next section.

Finally, for a given configuration which we are mapping onto the bead-spring model, we consider a relatively small number of chains, $M \sim O(10^2)$; it is not guaranteed that the resultant ensemble is representative of the underlying distribution. To mitigate this possibility, we generate a number of Monte Carlo realizations for which we calculate the local volume fractions $\bar{\varphi}_i(\mathbf{r})$ for comparison to the SCFT-based volume fractions. The lower the root-mean-square deviation $\mathrm{rms}^2=\Sigma_i \int dr(\bar{\varphi}_i(\mathbf{r})-\varphi_i(\mathbf{r}))^2$ for a given realization, the more representative we assume that configuration to be.

III. RESULTS AND DISCUSSION

A. Forward mapping

Determination of the SCFT parameters. To parametrize the SCFT model we need to determine two parameters: a statistical segment length a and an interaction parameter χN. The first of these can be determined from MD simulations of a pure homopolymer melt and reflects how many beads in the bead-necklace model comprise a statistical segment in the equivalent freely jointed (SCFT) chain. Specifically, we calculate the average squared radius of gyration $\langle R_g^2 \rangle$ for bead-necklace polymer chains obtained from MD simulations of homopolymer melts. Imposition of the constraint that the equivalent freely jointed chain has the same $\langle R_g^2 \rangle$ and contour length L_c as the bead-necklace chain in the melt, we obtain a pair of equations,

$$C_n n l^2 = 6\langle R_g^2 \rangle = Na^2, \quad nl = Na, \tag{10}$$

where C_n is the characteristic ratio of the bead-necklace chain (the subscript n here denotes that C_n can be molecular weight dependent for short chains) and l is a bond length equal to σ (=1.0 in this work). Equations (10) allow us to uniquely determine a and the number of statistical segments N in the equivalent freely jointed chain. In Table I, we report for each value of n the value of $\langle R_g^2 \rangle$ calculated from MD simulations and parameters for the equivalent freely jointed chain. Because of deviations from the n scaling of $\langle R_g^2 \rangle$ for small n (or, equivalently, the molecular-weight-dependent C_n), the segmental length a determined using Eqs. (10) indicates a slight molecular weight dependence. Figure 1 depicts the distributions of $\langle R_g^2 \rangle^{1/2}$ for a pure homopolymer melt as obtained from MD simulations of bead-necklace chains and SCFT calculations for equivalent freely jointed chains for three different molecular weights (using the conformational mapping described above and summarized in Table I). Unsurprisingly, the agreement is the poorest for the shortest chain length investigated ($n=19$ beads, $N=13$ segments). However, the agreement between the bead-necklace and equivalent freely jointed chains improves significantly with increasing molecular weight.

TABLE I. Parameters used to relate MD and SCFT calculations.

n	$\langle R_g^2 \rangle^{1/2}$	a	N	χN
19	2.18	1.500	12	2.46
28	2.73	1.578	18	3.80
38	3.21	1.627	23	4.25
57	3.97	1.667	34	7.60
76	4.64	1.695	45	8.67

In addition to the conformational mapping described above we must determine an effective interaction parameter χ or χN that adequately reproduces the interfacial properties in the equivalent homopolymer blend of freely jointed chains. Using bead-necklace MD simulation trajectories, normalized density profiles $\bar{\rho}^A(z)$ and $\bar{\rho}^B(z)$ were calculated.

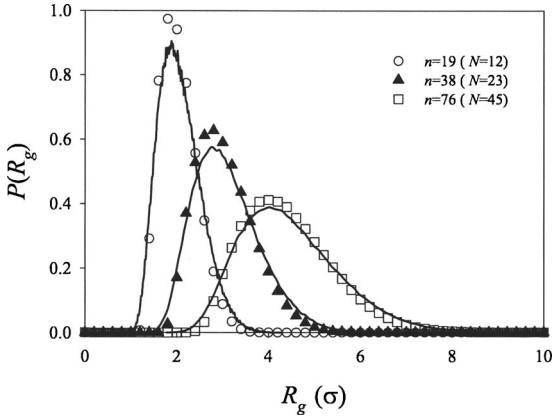

FIG. 1. Probability distribution of $(R_g^2)^{1/2}$ for bead-necklace chain (symbols) and equivalent freely jointed chain (lines) homopolymer melts as obtained from MD simulations and SCFT calculations, respectively.

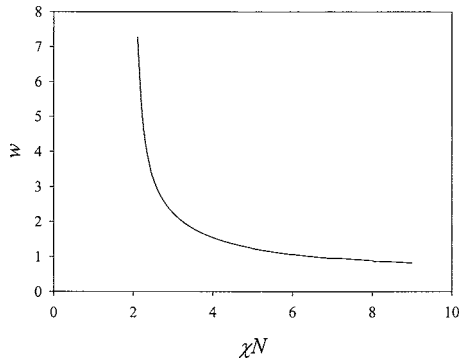

FIG. 2. Correlation between interfacial width (w) and interaction parameter χN in SCFT.

Normalization in the present context indicates that density profiles in the bulk phase (i.e., far from interface where profiles reach stable values) are set to zero and unity in the minority and majority phases, respectively,

$$\bar{\rho}^A(z) = \frac{\rho^A(z) - \rho^{A\text{in}B}_{\text{bulk}}}{|\rho^A_{\text{bulk}} - \rho^B_{\text{bulk}}|} \quad \bar{\rho}^B(z) = \frac{\rho^B(z) - \rho^{B\text{in}A}_{\text{bulk}}}{|\rho^A_{\text{bulk}} - \rho^B_{\text{bulk}}|}. \tag{11}$$

The quantities $\rho^A(z)$ and $\rho^B(z)$ in Eq. (11) are the intrinsic density profiles of beads A and B as a function of z, where the interface is assumed to correspond to $z=0$, $\rho^{A\text{in}B}_{\text{bulk}}$ and $\rho^{B\text{in}A}_{\text{bulk}}$ are values to which the intrinsic density profiles of the minority phases (A beads in the B-rich phase or *vice versa*) saturate in the bulk phase, and ρ^A_{bulk} and ρ^B_{bulk} are values of intrinsic density profiles to which the majority phases saturates in the bulk. Applying a well-established definition for the interfacial width,[26]

$$w = |\rho^A_{\text{bulk}} - \rho^{A\text{in}B}_{\text{bulk}}| \left(\frac{d\rho^A(z)}{dz} \right)^{-1}_{\rho^A(z)=\rho^B(z)}, \tag{12}$$

we can determine the interfacial width w for a homopolymer blend of bead-necklace chains. Note that, according to this definition of w, the interfacial width for a given blend system will be the same regardless of whether the normalized or un-normalized density profiles are used. Thus, Eq. (12) can also be used to define w in the SCFT calculations for the equivalent freely jointed chain blends if the density profiles are replaced with volume fraction profiles. In the SCFT approach, there is a unique correspondence between χN and w, as illustrated in Fig. 2 for the symmetric homopolymer blend. We can use this relationship to obtain a reliable prediction of the effective parameter χN for the equivalent freely jointed model in terms of the MD-based bead-necklace results.

In Fig. 3(a) we present normalized density profiles for blends obtained using the bead-necklace model (MD simulations) and corresponding volume fraction profiles obtained using the SCFT approach for the equivalent freely jointed chain blend employing a and χN parameters determined as described above. This figure clearly illustrates that the normalized bead density for the bead-necklace blend and volume fractions for the equivalent freely jointed chain blend are in excellent agreement. Figure 3(b) contains a comparison between the un-normalized density profiles for the bead-necklace model and the SCFT-based volume fraction profiles [in analogy to Fig. 3(a)]. For shorter chains, the bulk densities (volume fractions) resulting from the two methods are not the same when the interfacial width is chosen to match, indicating that the SCFT model is insufficient to describe simultaneously the interface (characterized by width parameter w) and the equilibrium compositions in the bulk. This failure of standard SCFT for short chains is not unexpected and has been observed experimentally.[27] For longer chains the bulk densities (volume fractions) are in good agreement, providing support for the proposed forward mapping procedure in that the two different features of the immiscible blend (interfacial width and bulk densities) are simultaneously in agreement after adjustment of the single parameter χN for practically interesting values of N. The chain length at which these two features are both well represented by SCFT gives us a gauge of when the forward mapping procedure is to be trusted.

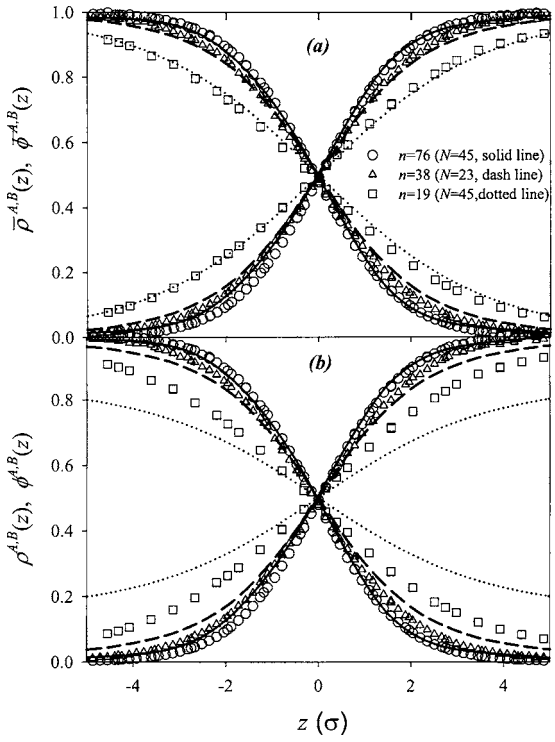

FIG. 3. Normalized (a) and un-normalized (b) density profiles for the homopolymer blends as obtained from MD simulations (symbols) and SCFT calculations (lines).

Using χN as an adjustable parameter for mapping between MD simulations (bead-necklace model) and SCFT (equivalent freely jointed chain model) is not justified if one takes the "theoretical definition" of χ as "…a strictly energetic quantity, defined in the spirit of regular solution theory by the exchange energy required to interchange two dissimilar monomers, divided by thermal energy k_BT."[28] We instead regard χ as an effective, free parameter, consistent with the experimental definition of "…a parameter obtained by fitting some experimental observations to a theoretical relation. As the experimental system is likely to violate one or more assumptions inherent in the theory, the resulting χ values reflect the influences of the various nonidealities present in

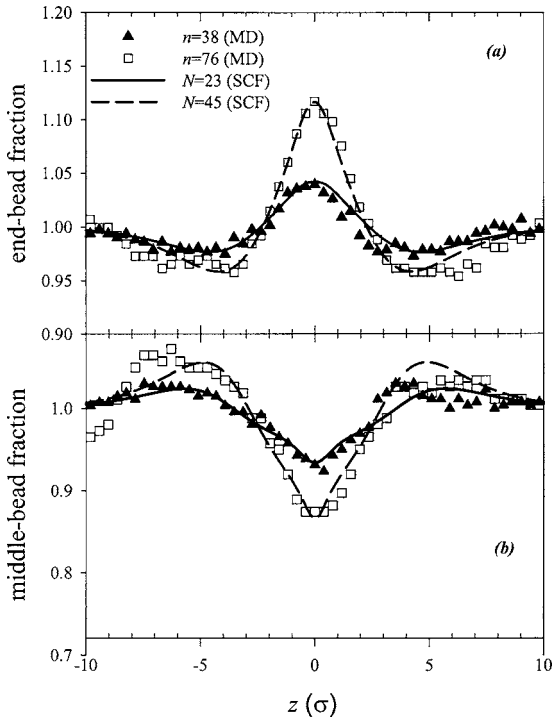

FIG. 4. Normalized fractions of (a) end and (b) middle beads/segments as a function of position from the interface as obtained from MD (symbols) and SCFT (lines).

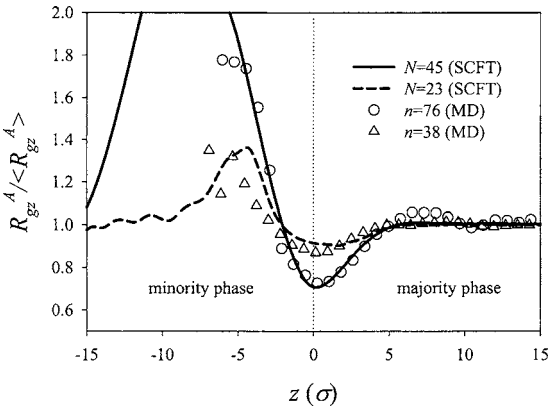

FIG. 5. Component R_g^z of chain radius of gyration as a function of position z from the interface. R_g^z is normalized by its bulk value. Symbols: MD simulations of bead-necklace blends; lines: SCFT predictions for equivalent freely jointed chain blends.

addition to the expected exchange energy contributions."[28] For any interfacial width w extracted from the MD bead-necklace simulations, a unique χN can be assigned that will yield the same profile in SCFT calculations for the equivalent freely jointed chain blend, provided that the chains are long enough so that the bulk densities agree, as discussed in the preceding paragraph. Obviously, there will be some uncertainty for each width w extracted from the MD simulations. This will translate into some uncertainty in χN. Uncertainties in χN will increase as the interfacial width w is decreased, for a specified absolute uncertainty in the latter parameter. Unfortunately, this large error zone (regions in Fig. 2 corresponding to smaller widths) will occur for longer chains, which is precisely the region where the forward mapping should work best. Although we have not done a rigorous error analysis here, this potential difficulty is mitigated by thoroughly equilibrating and sampling the bead-necklace blends, thereby minimizing the error in w. Further, limited uncertainties in χN do not present a serious problem, since the interfacial characteristics (width and bulk density) saturate for larger χN values, as can be seen in Figs. 2 and 3, respectively.

Structural properties. It is important to demonstrate that our approach for fitting the parameters required by SCFT adequately reproduces the main structural and conformational features predicted for the bead-necklace polymer blends. The first quantities we compare are the fractions of end and middle groups of chains along the z direction. In Fig. 4 we show these results plotted as a function of z for two blend systems, normalized by the average fraction of the beads of that type in the system, as obtained directly from MD simulations and from SCFT using forward-mapped parameters. Fraction values greater than unity indicate a local excess of beads of a given type (i.e., end or middle) relative to their average fraction in the overall system; similarly, values less than unity are indicative of local depletion. As expected, the end beads exhibit an increased probability near the interface [Fig. 4(a)], due to a lower entropy penalty for end groups in this region relative to that for beads interior to the chain, for which depletion occurs near the interface [Fig. 4(b)]. The effect becomes more pronounced with increasing molecular weight. Figure 4 clearly illustrates that our approach to parametrize SCFT based on MD results for specific chemical interactions yields accurate predictions of end- and middle-bead number density profiles, including the molecular weight dependence of these quantities.

B. Reverse mapping

Conformational properties. A first check on the configurations generated from SCFT by density-biased Monte Carlo is to compare conformational features calculated from MD using the bead-necklace model. In Fig. 5, the z component of chain radius of gyration R_g^z, normalized by the system average of this property $\langle R_g^z \rangle$, is plotted with respect to individual chain center-of-mass positions along the z direction. It is expected that chains tend to become flattened or "pancaked" near the interface in the direction parallel to the interface, and this is corroborated here for both the MD- and SCFT-based results. This figure clearly illustrates that, passing from the bulk in the majority phase toward the interface, R_g^z for those "majority" chains decreases, passes through a minimum centered at the interface, and then increases as the chains of this type become the minority phase. The statistical uncertainty for the data in the minority region is large, especially for the MD simulation results; however, MD simulations and SCFT calculations agree well in the majority phase and near the interface in the minority region, for all molecular weights investigated. For both systems the amplitude of the effect and its persistence away from $z=0$ increase with increasing molecular weight.

Procedure for mapping a freely jointed chain onto a bead-necklace chain. For each chain in the ensemble gener-

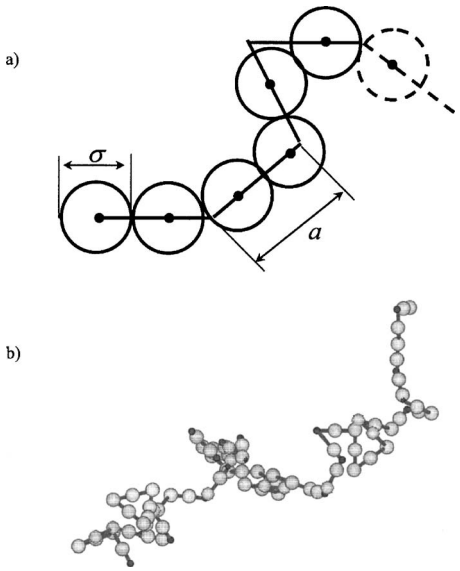

FIG. 6. (a) Schematic illustration of the reverse mapping of a freely jointed chain (defined by solid line segments) onto the equivalent bead-necklace model chain (large circles) with bead centers (small filled circles) positioned along the contour of the freely jointed chain. (b) Snapshot of an $N=45$ freely jointed chain and the corresponding $n=76$ bead-necklace chain.

ated from an SCFT density-biased Monte Carlo realization, we distribute n beads of the bead-necklace chain along the contour of the equivalent freely jointed chain (defined by N segments). The first bead of each bead-necklace chain is positioned to coincide with the starting point of the first segment. The next step is to determine whether the second bead (separated from the first bead by a bond of fixed length σ) can be placed between the beginnings of the first and second segments along the bond (of fixed length a) connecting them. (We emphasize that the SCFT segment length a and MD bead diameter σ are different; for $n=76$, $a=1.695\sigma$.) If this condition is satisfied we place the second bead in that position along the vector separating segments 1 and 2 and proceed to the next bead. If a given bead $i+1$ cannot be placed on the same segmental bond as the ith bead, then we place the $(i+1)$th bead on the next segmental bond such that the distance between beads i and $i+1$ is still σ [see illustration in Fig. 6(a)]. Due to this last step, which "cuts the corner," it would be fortuitous if the mapping protocol should yield an exact match between contour lengths for N segments and n beads. Thus, we developed an iterative procedure to achieve an acceptable mapping between segmental and bead-level descriptions of the system. Specifically, if the nth bead does not lie on the Nth segment, we scale that bead's diameter σ by 1% (increasing or decreasing σ depending on the direction of the mismatch). Further, we allow beads to be placed outside the segmental bond (yet still along the direction of that bond), allowing 1% change in the segmental bond length a per iteration. This procedure was repeated until exactly n beads were mapped onto N segments, for each chain in turn. The largest observed deviation from the base line bead diameter was 0.1σ, while the largest extension outside segmental bond was $0.06a$. A snapshot illustrating a bead-necklace chain mapped onto a freely jointed SCFT chain is shown in Fig. 6(b).

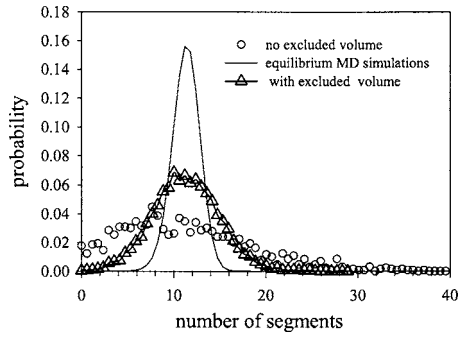

FIG. 7. Probability distribution for statistical segments in a subvolume of size of $3\sigma\times3\sigma\times3\sigma$.

The 20 "most representative" configurations (i.e., those 20 characterized by the smallest mean-squared deviation between local volume fractions $\bar{\varphi}_i(\mathbf{r})$ predicted using SCFT and from the density-biased Monte Carlo sampling based on 200 realizations) were generated for the largest molecular weight investigated ($N=45$ segments) and $\chi N=8.67$. (Refer to Sec. II D.) Each configuration consisted of 328 freely jointed chains in a three dimensional periodic, orthorhombic cell with dimensions $15\times15\times157$ (in units of σ). These freely jointed chain blend melt configurations were reverse mapped to the corresponding bead-necklace systems for $n=76$ beads.

Configuration relaxation. The generation of a melt as described in Sec. II D and the preceding paragraphs results in a significant amount of aphysical overlap between beads. To resolve this, we performed short MD simulations of the reverse-mapped configurations with imposed distance-based upper bounds on bead-bead interaction energy and force magnitudes. In these simulations, if two beads were found to be closer than some distance r_s, their interaction energy and force were assigned to be equal to the corresponding values for $r=r_s$, thereby eliminating the large, numerically unstable repulsive forces associated with such contacts. During the first 1000 integration steps of this relaxation stage, we also rescaled the velocities of all beads at every time step to enforce the system total kinetic energy corresponding to the desired temperature. This protocol was sufficient to remove most of the excess potential energy due to initial bead-bead overlap. The SHAKE algorithm was used to constrain bond length to σ. Small deviations of the bond length from σ allowed during reverse mapping procedure were corrected by SHAKE at the first integration step. Following 1000 initial integration steps, the relaxation MD simulation continued for another 30 000 steps in the NVT ensemble. Similar procedures have been employed previously in simulations of homopolymer[25] and block copolymer melts.[10,11]

While the general procedure described above is anticipated to work for dense polymer melts, it was shown in a recent study of homopolymer melts,[24] as well as in the present simulations, that it has a significant drawback. To illustrate this we have calculated the local density of segments in the SCFT-based density-biased Monte Carlo freely jointed chain configurations. In Fig. 7 we show the distribution of the number of segments in a cubic subvolume of size $(3\sigma\times3\sigma\times3\sigma)$, calculated from configurations generated without inclusion of any excluded volume interactions and

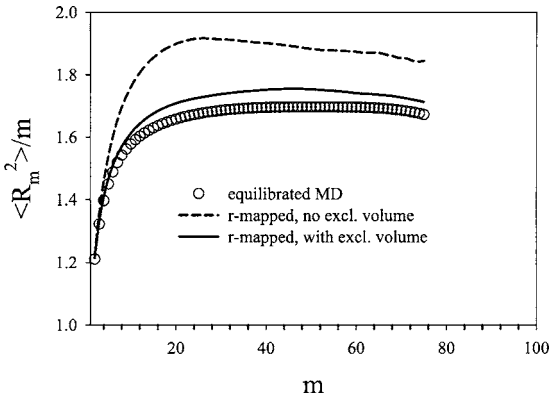

FIG. 8. $\langle R_m^2 \rangle / m$ as a function of m as obtained from well equilibrated MD simulations, reverse-mapped (with and without excluded volume interactions), and relaxed configurations.

from a fully equilibrated MD simulation run of the corresponding bead-necklace model. In the equilibrium MD simulation, the number of statistical segments (calculated as number of beads divided by a) per subvolume is Gaussian distributed around $N_s \sim 11$. By contrast, the distribution from the configurations obtained by reverse mapping is much broader, with significant probability of both empty and densely filled subvolumes; that is, the simple reverse mapping procedure yields inappropriately large inhomogeneities in the system.

The 1000 step MD relaxation protocol for reverse-mapped bead-necklace chain configurations results in the "pushing away" of beads that are located in high density regions towards low density regions, leading to a more homogeneous number density distribution within the system. However, it also results in the "stretching" of the chains on intermediate length scales. To illustrate this we have calculated the average intramolecular mean-squared distance $\langle R_m^2 \rangle$ between the ith and $(i+m)$th beads, normalized by m. In the limit of large m, $\langle R_m^2 \rangle / m$ should be equal to a, while for small m the non-Gaussian nature of the bead-necklace model on short length scales leads to $\langle R_m^2 \rangle / m < a$. In Fig. 8 we compare results for $\langle R_m^2 \rangle / m$ obtained from a well equilibrated MD simulation of a blend comprised of 328 chains of length $n=76$ (open circles) to those obtained from 20 reverse-mapped configurations, as defined earlier, after relaxation (1000 steps of overlap-removal MD plus 30 000 steps of *NVT*-MD) that were reversed mapped from the most representative freely jointed chain configurations (circles), as defined earlier. As was observed previously for homopolymer melts,[24] we find that the largest perturbation of chain dimensions characterized by $\langle R_m^2 \rangle / m$ occurs at intermediate length scales, $m \sim 20-30$. Note that, depending on parameters and procedural details of the relaxation MD phase (e.g., values of r_s and length of the initial bounded force equilibration run), one can in principle obtain configurations with very reasonable average global chain conformations (e.g., an average radius of gyration within a few percent of the expected value or, equivalently, $\langle R_m^2 \rangle / m$ equal to a for $m=n$), but that deviations on the intermediate length scales still arise for all such variations of the protocol. Moreover, in order to relax these perturbations on the m-bead length scale, it is not sufficient to continue MD equilibration of the system over time scales required for relaxation of an m-bead long polymer melt.[24] Rather, a full relaxation of the melt is necessary to eliminate these intermediate-scale perturbations. Therefore, if one uses the method outlined above for the creation of long, entangled polymer melt configurations, complete relaxation of the system on all length scales might not be achievable.

To overcome this bottleneck in the mapping between ideal chains (i.e., freely jointed chains) and chemically realistic (i.e., bead-spring) chains Auhl *et al.* have employed additional MC density homogenization procedures in combination with a double-bridging algorithm.[24] We have adopted a simpler protocol that is described below.

Excluded volume density-biased MC approach. In our approach we partially include the excluded volume interactions during the density-biased Monte Carlo generation of the freely jointed chain configurations in the melt. When the ith segment of the kth chain is generated, it "feels," in addition to the SCFT fields, the excluded volume interactions of all other segments (except for some number N_{excl} of adjacent intramolecular neighbors). Each segment in this procedure is represented by a hard sphere of radius r_{excl}. If a trial placement of a given segment overlaps with any other segment (over the set of all intermolecular segments and intramolecular ones separated by more than N_{excl} segments) then the attempt is rejected and another placement is attempted. We have restricted N_{excl} 4. The exclusion of N_{excl} intramolecular neighbors is motivated by the fact that the intramolecular overlap on such local scales is not important and can be easily annealed during the relaxation MD simulation run. One might expect that the inclusion of these excluded volume interactions during the density-biased MC procedure will affect overall chain conformations relative to the case of zero excluded volume. However, allowing local overlap minimizes this effect. Therefore, by adjusting the two (practically empirical) parameters N_{excl} and r_{excl}, one can, in principle, obtain both the desired chain dimensions and a suitably homogeneous distribution of segments within the system.

Another important issue to consider in this procedure is that when the first freely jointed chain is placed in the simulation cell in the density-biased MC procedure, it (obviously) is not subject to excluded interactions with other chains, whereas the final chain in the configuration will be subject to excluded volume interaction with all chains previously generated. This certainly creates a dependence of the chain conformational properties (e.g., radius of gyration) on when in the sequence of chain generation a given chain is placed. Thus, while the average radius of gyration in a given situation can be "tuned" using N_{excl} and r_{excl}, the radius of gyration for individual chains will likely have an "index dependence," specifically, increased values of R_g for chains with low index and reduced values for chains with high index. To circumvent this possibility, we initially generate M chains (total number of chains in the configuration), then eliminate the first chain and generate an $(M+1)$th one, then eliminate the second chain and generate an $(M+2)$th one, and so on until the first M chains are replaced by another M chains

(indexed as $M+1$ to $2M$). By doing this the M final chains are generated in an essentially even-handed fashion.

To determine optimal values for N_{excl} and r_{excl}, we focused on the $n=38$ ($N=23$) system. In this low molecular weight regime, the equilibrium chain dimensions on all length scales can be easily obtained from MD simulations. Therefore N_{excl} and r_{excl} can be determined such that the freely jointed chains and subsequently reverse-mapped bead-necklace chains are in near-perfect agreement with the conformational characteristics of bead-necklace chains obtained directly from molecular dynamics. We found that $N_{\text{excl}}=4$ and $r_{\text{excl}}=0.29\sigma$ yield accurate matches between reverse-mapped and equilibrium bead-necklace chains for the conformational properties on all length scales. These parameters, while empirical and adjusted for $n=38$ chains, are apparently universal for all larger molecular weights. This is evident in Fig. 8, where we show $\langle R_m^2\rangle/m$ for reverse-mapped and relaxed configurations for chains with $n=76$ using N_{excl} and r_{excl} determined for the $n=38$ system. No significant perturbation of chain configurations is observed on any length scale. The generation of systems with even longer chains ($n=304$) also did not exhibit deviations from the $\langle R_m^2\rangle/m$ master curve. Examination of the distribution of the number of segments in $3\sigma\times3\sigma\times3\sigma$ subvolumes for configurations generated using density-biased Monte Carlo with partial excluded volume interactions indicates a significant improvement relative to configurations generated without excluded volume (Fig. 7, triangles). Although $r_{\text{excl}}=0.29\sigma$ is small compared to "real" segment dimensions ($a=1.7\sigma$ for long chains), it leads to significant narrowing of the distribution of the number of segments in subvolumes and hence noticeable homogenization of the segmental density in the system. Note that the primary reason for perturbed configurations in the unmodified approach of Sec. II D is not the intrinsic overlap of the mapped beads but rather their heterogeneous distribution (or incorrect intermolecular correlations) in the initial configurations. As the results above illustrate, if this heterogeneity is reduced then bead overlap on very short length scales can be easily relaxed on short time scales without perturbation of chain conformations on larger length scales.

To ensure that a 30 000 step MD relaxation run is sufficient to completely remove any excess energy introduced initially due to the overlap of beads during chain generation, we have monitored the evolution of the average energy per bead (total energy of the system normalized by number of beads in the system) during the run. The results are shown in Fig. 9 for $n=76$, where one can see that within 10 000 integration steps the energy reaches a steady-fluctuating value, indicating that the chosen duration of the relaxation run is sufficient. To confirm that the interfacial properties of reverse-mapped configurations are representative for the system of interest we compare in Fig. 10 A and B phase density profiles and fraction of end beads [panels (a) and (b), respectively] along the z direction as obtained from well equilibrated MD simulations to those of the 20 "best" reverse-mapped/relaxed configurations. While the statistics averaged over single snapshots from 20 reverse-mapped configurations are noisy, it is clear that the interfacial properties in reverse-mapped configurations are accurate.

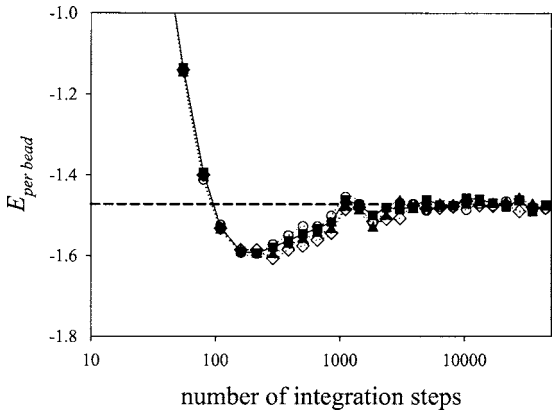

FIG. 9. Time evolution of the average energy per bead for four reverse-mapped bead-necklace configurations during relaxation MD simulations. Horizontal line indicates the average value obtained from well equilibrated MD simulations.

IV. CONCLUSIONS

We have developed a bidirectional mapping procedure for homopolymer blends that links molecular dynamics simulations and self-consistent field theory (SCFT). In the "forward" direction molecular dynamics is used to generate well equilibrated interfacial density profiles for bead-necklace systems, for chain molecular weights that can be successfully relaxed using standard methods. Enforcing the constraint that the average squared radius of gyration $\langle R_g^2\rangle$ and contour length C_n are the same for the bead-necklace molecular dynamics chains and freely jointed chains invoked in the SCFT yields well-defined relationships between the

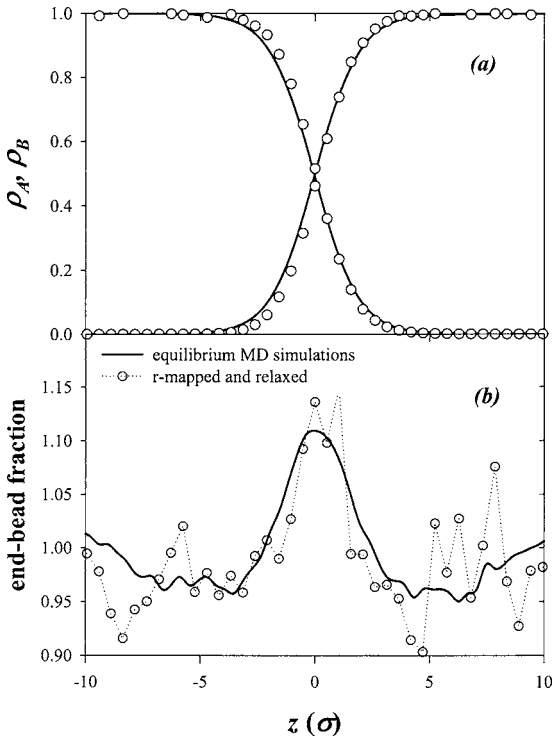

FIG. 10. (a) A and B phase density profiles and (b) fraction of end beads along z direction as obtained from well equilibrated MD simulations (line) and from reverse mapped with excluded volume interactions and subsequently relaxed configurations.

number of molecular dynamics beads n and statistical segments N and bead diameter σ and statistical segment length a. This information is used to determine an effective "Flory-Huggins" interaction strength χN that is the only free parameter appearing in the version of SCFT used here.

In the "reverse" direction, a density-biased Monte Carlo approach is used in conjunction with the calculated density fields from SCFT to generate representative chain configurations in the blend, based on freely jointed chains that include limited excluded volume interactions for all intermolecular contacts and for intramolecular length scales in excess of a specified minimum value. The partial excluded volume interaction is characterized by two empirical parameters r_{excl} and N_{excl} that can be optimized by comparison to MD simulation results for well equilibrated, short chain blends. Mapping of the freely jointed chains thus obtained onto bead-necklace chains suitable for use in molecular dynamics simulations is performed using an efficient iterative procedure based on the relationships between n and N and σ and a mentioned in the preceding paragraph.

A straightforward MD equilibration protocol is used to relax initial bead-bead overlaps that result from reverse mapping procedure. Specifically, a very short trajectory segment (1000 time steps in this work), during which the large forces due to initial bead overlap are restricted to numerically manageable values and velocities are scaled to yield the desired temperature at every time step, is followed by a short standard *NVT*-MD segment (30 000 time steps in this work). These short trajectory segments were found to be sufficient to gracefully remove initial overlaps, yield distributions of monomer densities in subvolumes that are in reasonable agreement with results from long MD runs, and provide stable system energies that agree well with long time MD simulation results. Subsequent to this efficient equilibration protocol, system configurations are suitable for long production runs.

In addition to the correspondence of the number density distributions and energies mentioned in the preceding paragraph, the bidirectional approach was further validated by comparisons of the following properties, as obtained directly from well equilibrated MD runs and from the reverse mapping procedure, generally over a range of chain lengths accessible to molecular dynamics (i.e., below the entanglement molecular weight): (1) interfacial density profiles; (2) distributions of "end" and "middle" groups in the vicinity of the interface; and (3) normalized z component of chain radius of gyration in the bulk majority phase, at the interface, and in the minority phase. In addition, we have demonstrated that the method yields the correct chain conformations on all length scales based on the behavior of $\langle R_m^2/m \rangle$, even for chain lengths well above the entanglement molecular weight. This latter point is a strong indicator of the validity and usefulness of the bidirectional mapping procedure described. An interesting question is the efficacy of this approach, subject to modest alterations, in the generation of initial equilibrium configurations for complex morphologies in microphase separated block copolymer systems.

ACKNOWLEDGMENTS

This work was supported by the Los Alamos National Laboratory Exploratory Research component of the Laboratory Directed Research and Development program. This work was carried out under the auspices of the National Nuclear Security Administration of the U.S. Department of Energy at Los Alamos National Laboratory under Contract No. DE-AC52–06NA25396.

[1] F. S. Bates and G. H. Fredrickson, Annu. Rev. Phys. Chem. **41**, 525 (1990).
[2] J. Baschnagel, K. Binder, P. Doruker *et al.*, Adv. Polym. Sci. **152**, 41 (2000).
[3] K. Kremer, *Multiscale Modeling and Simulation* (Springer, Berlin, 2004), p. 105.
[4] E. Jaramillo, D. T. Wu, G. S. Grest, and J. G. Curro, J. Chem. Phys. **120**, 8883 (2004).
[5] T. C. Clancy and W. L. Mattice, J. Chem. Phys. **112**, 10049 (2000).
[6] K. Binder and A. Milchev, J. Comput.-Aided Mol. Des. **9**, 33 (2002).
[7] K. Binder, Comput. Phys. Commun. **147**, 22 (2002).
[8] M. W. Matsen and M. Schick, Phys. Rev. Lett. **72**, 2660 (1994).
[9] For definiteness, we regard "verification" as ensuring correct solutions to the relevant equations and "validation" as proof that the equations solved are appropriate based on comparison to experiment.
[10] T. Aoyagi, T. Honda, and M. Doi, J. Chem. Phys. **117**, 8153 (2002).
[11] T. Aoyagi, F. Sawa, T. Shoji, H. Fukunaga, J. Takimoto, and M. Doi, Comput. Phys. Commun. **145**, 267 (2002).
[12] A. F. Terzis, D. N. Theodorou, and A. Stroeks, Macromolecules **33**, 1397 (2000).
[13] See, for example, Refs. 4–7.
[14] G. Milano and F. Müller-Plathe, J. Phys. Chem. B **109**, 18609 (2005).
[15] G. Santangelo, A. Di Matteo, F. Müller-Plathe, and G. Milano, J. Phys. Chem. B **111**, 2765 (2007).
[16] M. Doi and S. F. Edwards, *The Theory of Polymer Dynamics* (Claredon, Oxford, 1986).
[17] B. J. Palmer, J. Comput. Phys. **104**, 470 (1993).
[18] G. J. Martyna, M. E. Tuckerman, D. J. Tobias, and M. L. Klein, Mol. Phys. **87**, 1117 (1996).
[19] M. W. Matsen, J. Phys.: Condens. Matter **14**, R21 (2002), and references therein.
[20] G. H. Fredrickson, V. Ganesan, and F. Drolet, Macromolecules **35**, 16 (2002).
[21] F. Drolet and G. H. Fredrickson, Phys. Rev. Lett. **83**, 4317 (1999).
[22] G. Tzeremes, K. Ø. Rasmussen, T. Lookman, and A. Saxena, Phys. Rev. E **65**, 041806 (2002).
[23] K. Ø. Rasmussen and G. Kalosakas, J. Polym. Sci., Part B: Polym. Phys. **40**, 1777 (2002).
[24] R. Auhl, R. Everaers, G. S. Grest, K. Kremer, and S. J. Plimpton, J. Chem. Phys. **119**, 12718 (2003).
[25] K. Kremer and G. S. Grest, J. Chem. Phys. **92**, 5057 (1990); M. Putz, K. Kremer, and G. S. Grest, Europhys. Lett. **49**, 735 (2000).
[26] M. W. Matsen and M. Schick, Macromolecules **27**, 187 (1994).
[27] M. Sferrazza, C. Xiao, D. G. Bucknall, and R. A. L. Jones, J. Phys.: Condens. Matter **13**, 10269 (2001).
[28] T. P. Lodge, Macromol. Chem. Phys. **204**, 265 (2003).